Bed load motion and grain sorting in a meandering stream

Charriage et fractionnement dans une rivière à méandres

PIERRE Y. JULIEN, *Department of Civil Engineering, Engineering Research Center, Colorado State University, Fort Collins, CO 80523, USA*

DEBORAH J. ANTHONY, *Department of Earth Resources, Colorado State University, Fort Collins, CO 80523, USA*

ABSTRACT

A three-dimensional moment analysis defines both particle mobility and the average orientation angle of moving bedload particles in meander bends. Accordingly, under identical bed shear stress and near-bed streamline orientation angle on a side slope, bedload particles of different sizes move in different directions. This sorting mechanism has been verified in the sharp meander bends of Fall River, Colorado. The extensive field data set includes near-bed sediment transport measurements by size fractions from 0.125 to 32 mm using a Helley-Smith sampler. The field measurements in two meander bends corroborate the theoretical model: particles finer than d_{50} preferentially move up the point bar and particles coarser than d_{50} move toward the thalweg. The measured deviation angle between the mean trajectory of 0.125 mm and 32 mm particles reaches 20° near the bend apex.

RÉSUMÉ

Une analyse tri-dimensionnelle des moments de force sur une particule définit la mobilité et l'angle de déplacement des particules en charriage dans une rivière à méandres. Sous une contraine de cisaillement donnée, les particules sur un plan incliné se déplacent dans différentes directions selon leur taille. Il en résulte un mécanisme de ségrégation qui a été vérifié dans les méandres de la rivière Fall au Colorado. Les données in-situ incluent le transport de sédiment avec l'échantillonneur Helley-Smith pour les particules dont la taille varie entre 0.125 et 32 mm. Les mesures in-situ corroborent le modèle théorique: les particules plus fines que le d_{50} se déplacent préférentiellement vers la berge convexe tandis que les particules de taille excédant le d_{50} se déplacent vers le thalweg. L'angle de déviation entre la trajectoire mediane des particules de 0.125 mm et de 32 mm atteint 20° près du point de courbure maximale.

Key Words: Point bars, river bends, particle stability, secondary flow, sediment deposits

1. Introduction

Particle stability in alluvial channels depends on a combination of gravitational and hydrodynamic forces applied on individual particles. Incipient motion of bed sediment particles has been studied by DuBoys (1879), Shields (1936), and Yalin and Karahan (1979), among many others. Shields' contribution clearly stands out because of the physical significance of the grain shear Reynolds number Re^* which describes the ratio of grain size to the laminar sublayer thickness. Earlier methods strictly applicable to uniform bed material have been extended to graded sediment mixtures by Egiazaroff (1965), Hayashi et al. (1980), and Kuhnle (1993) among others.

For downstream flow along side slopes, the analyses of Lane (1953) and Brooks (1963) considerably improved upon earlier findings in using two-dimensional forces applied to particles. Two-dimensional sediment transport has been considered by Engelund (1974), Koch and Flokstra (1980), Ikeda (1982), and Kovacs and Parker (1995), with applications to curved open channels by Odgaard (1982), Parker and Andrews (1985), Dietrich and Whiting (1989), Whiting and Dietrich (1990), and others.

Odgaard (1981) analyzed the transverse bed slope and the bed surface characteristics. He assumed that under equilibrium conditions, the sediment particles shaping the bed surface are statically stable in both radial and longitudinal directions, but at impending motion in the longitudinal direction only. Struiksma et al. (1985) calculated the sediment transport direction angle according to the formula of van Bendegom with a weight function $F(\tau_*) = f_s \tau_*$ where τ_* is the Shields parameter and the correction factor $1<f_s<2$. Recent investigations of the weight function by Talmon et al. (1995) suggest $F(\tau_*) = 1.7\sqrt{\tau_*}$ for laboratory conditions and $F(\tau_*) = 0.85\sqrt{\tau_*}$ for field conditions. They concluded that a distinction should be made between laboratory conditions and natural rivers, and that the transverse slope effect seems dependent on the ratio of grain diameter to flow depth. Bed topography and transverse sediment sorting in a channel bend were investigated by Yen and Lee (1995) under unsteady flow conditions with non-uniform sediment. An unsteady flow parameter may also influence bed deformation and sediment sorting.

Earlier models based on force equilibrium included a coefficient of dynamic Coulomb friction. It became clear in Parker and Andrews (1985) that bedload transport alone could not accomplish sorting when the Coulomb coefficient remained constant because the angle between the direction of bedload transport and the downstream direction is independent of grain size. Sorting could either be explained by: 1) distinct consideration of bedload and suspended load given different angles between the direction of fluid bed shear stress and the downstream direction; or 2) differential values of the hiding function for different sizes of a sediment mixture. Instead of using the sum of forces to describe particle stability, Stevens and Simons (1971) developed a two-dimensional moment analysis to determine the stability of riprap. The method has been extended to three dimensions by Julien (1995), and provides the orientation angle of moving particles, which is

Revision received January 3, 2001. Open for discussion till August 31, 2002.

the primary interest of this paper. The method has been tested with laboratory data by Kawai and Julien (1996). The analysis indicates that the size of point bars depends on particle size.

The objective of this study is to examine the applicability of this method for sediment transport by size fractions in natural meander bends. The foregoing analysis focuses on the average direction angle of bedload particles for different size fractions. The three-dimensional particle stability analysis in Section 2 is followed by a description of the sharp meander bends of Fall River, Colorado in Section 3. In Section 4, apex/crossing differences in terms of calculated bedload direction are then compared with field measurements of bedload sediment transport by size fractions.

2. Three-dimensional particle stability analysis

Figure 1 illustrates the forces acting on a cohesionless particle resting on an embankment inclined at a side slope angle Θ_1, and a downstream bed slope angle Θ_0. These are the lift force F_L, the drag force F_D, the buoyancy force F_B, and the weight of the particle F_W. As long as the water surface slope in the downstream direction is small, the buoyancy force can be subtracted from the particle weight to give the submerged weight $F_S=F_W-F_B$. The lift force is defined as the fluid force normal to the embankment plane whereas the drag force is acting along the plane in the same direction as the velocity field surrounding the particle.

For notational convenience, one defines two geometrical parameters a_Θ and $\tan\Theta$ from the side slope angle Θ_1 and the downstream bed slope angle Θ_0. These two parameters describe the projection of the submerged weight vector along the embankment plane. The angle Θ is obtained from the ratio of the two projection components of F_S in the embankment plane as

$\tan\Theta = \dfrac{\cos\Theta_1 \sin\Theta_0}{\cos\Theta_0 \sin\Theta_1}$, which can be approximated by

$\tan\Theta \cong \dfrac{\sin\Theta_0}{\sin\Theta_1}$ as long as both angles are fairly small (less than about 20°). The fraction of the submerged weight that is normal to the embankment plane is given by

$a_\Theta = \sqrt{1 - \cos^2\Theta_0 \sin^2\Theta_1 - \cos^2\Theta_1 \sin^2\Theta_0}$, which is approximated by $a_\Theta \cong \sqrt{\cos^2\Theta_1 - \sin^2\Theta_0}$ when both angles are small (less than about 20°). As a realistic approximation, the submerged weight has one sideslope component $F_S \sin\Theta_1$, one downslope component $F_S \sin\Theta_0$, and a component normal to the plane $F_S a_\Theta$, as shown in Figure 1. The streamline deviates from the downstream direction at an angle λ along the embankment plane (λ is defined positive downward). Once in motion, the particle follows a direction at an angle β from the direction of steepest descent. A particle moves along the horizontal when $\beta=90°$ and moves in the downstream direction when $\beta+\Theta=90°$. When $\beta+\Theta>90°$, a particle moves up the side slope toward the free surface. Conversely, when $\beta+\Theta<90°$, a particle moves down the side slope toward the thalweg. In most streams, the downstream slope Θ_0 will be sufficiently small to consider that $\Theta\cong 0$ and $\mathbf{a_\Theta \cong \cos\Theta_1}$. The downstream direction thus practically corresponds to $\beta=90°$, values of $\beta<90°$ indicate particles moving toward the thalweg, and $\beta>90°$ indicates motion toward the free surface.

Stability against rotation of a particle determines incipient motion when the equilibrium of moments about the point of rotation is satisfied. The deviation angle δ is measured between the streamline and the particle direction. The angles δ and β , and the moment arms ℓ_1, ℓ_2, ℓ_3 and ℓ_4 are shown in Figure 1. For instance, stability about point 0 corresponds to:

$$l_2 F_S a_\Theta = l_1 F_S \sqrt{1 - a_\Theta^2} \cos\beta + l_3 F_D \cos\delta + l_4 F_L \qquad (1)$$

The left-hand side of (1) defines the stabilizing moment due to the particle weight. Clearly the last term on the right-hand side of (1) denotes the lift moment, which always destabilizes the particle. The first two terms on the right-hand side of (1) determine about which pivot point particle P is to rotate. In most cases, their net sum is positive, and moments about 0 are considered. Should their net sum be negative, when $\lambda<0$, the particle will then rotate about point 0′ instead of 0.

The stability factor SF_0 , for rotation about point 0 is defined as the ratio of the resisting moments to the moments generating motion. In the case shown in Figure 1 where both $\cos\delta$ and $\cos\beta$ are positive, the stability factor SF_0 is the ratio of the sum of counter clockwise moments about 0 to the sum of clockwise moments about 0, thus

$$SF_0 = \frac{\wedge_2 F_S a_\Theta}{\wedge_1 F_S \sqrt{1-a_\Theta^2} \cos\beta + \wedge_3 F_D \cos\delta + \wedge_4 F_L} \qquad (2)$$

Notice that each term in (2) must be positive, otherwise the formulation for SF_0 is changed to express the ratio of positive stabilizing moments to the sum of positive destabilizing moments.

Because the stability factor SF_0 equals unity when the angle Θ_0, or Θ_1, equals the angle of repose ϕ under static fluid conditions ($F_D=F_L=0$), it is found that $\tan\phi=\ell_2/\ell_1$. Dividing both the numerator and the denominator by $\ell_1 F_S$, transforms (2) into:

$$SF_0 = \frac{a_\Theta \tan\phi}{\eta_1 \tan\phi + \sqrt{1-a_\Theta^2}\cos\beta} \qquad (3)$$

in which, $\eta_1=M+N\cos\delta$ after defining

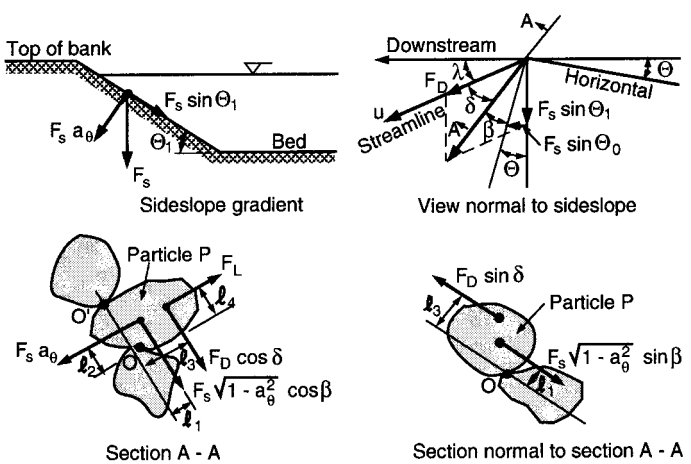

Fig. 1 Moment stability analysis of a particle

$$M = \frac{\wedge_4 F_L}{\wedge_2 F_S};\ \text{and}\ N = \frac{\wedge_3 F_D}{\wedge_2 F_S}$$

The parameter M/N represents the ratio of lift to drag moments of force. The case of no lift is given by M/N=0 and equal moments are described by M=N or (M+N)/N=2. The variable η_1 is called the side slope stability number for the particle on the embankment. The variable η_1 relates to the stability number η_0=M+N for particles on a plane horizontal surface ($\Theta_0=\Theta_1=\delta=0$) after considering $\lambda+\delta+\beta+\Theta=90°$:

$$\eta_1 = \eta_0 \left\{ \frac{(M/N) + \sin(\lambda+\beta+\Theta)}{1+(M/N)} \right\} \tag{4}$$

and

$$\eta_0 = \frac{\tau_o}{\tau_c} = \frac{\tau_o}{(G-1)\rho\, g\, d_s\, \tau_{*c}} \tag{5}$$

The stability number η_0 is calculated from the applied shear stress τ_o, the critical shear stress on a plane horizontal surface τ_c, the particle diameter d_s, the mass density of the particle $\rho_s=G\rho$, the mass density of the fluid ρ, the gravitational acceleration g, and the critical value of the Shields parameter τ_{*c}.

This normalized form of the Shields parameter shows that $\eta_0=1$ describes incipient motion of particles on a plane horizontal bed. When the flow is fully turbulent over a hydraulically rough horizontal surface, incipient motion approximately corresponds to $\tau_{*c}\cong 0.047$ and $SF_0=\eta_0=1$.

The second equilibrium condition indicates the direction of a moving particle from equilibrium conditions along the section normal to A-A in Figure 1:

$$\wedge_3 F_D \sin\delta = \wedge_1 F_S \sqrt{1-a^2_\Theta}\, \sin\beta \tag{6}$$

After writing δ as a function of λ, Θ and β, solving for β gives

$$\beta = \tan^{-1}\left\{ \frac{\cos(\lambda+\Theta)}{\frac{(M+N)\sqrt{1-a^2_\Theta}}{N\eta_0\tan\phi} + \sin(\lambda+\Theta)} \right\} \tag{7}$$

The angle β determines the direction of motion of a sediment particle in contact with the inclined plane. The particle orientation angle depends on: 1) surface topography via Θ and a_Θ; 2) stream flow direction at an angle λ; and 3) particle characteristics such as angle of repose ϕ, and excess shear $\eta_o=\tau_o/\tau_c$. A complete calculation example is given in Appendix I.

In nature, meandering streams consist of curved channels with the apex corresponding to the cross-section with minimum radius of curvature, separated by somewhat rectilinear crossings. The bed elevation at crossings is fairly horizontal compared to the steeper side slopes typical of point bars located alongside the inner bank near the apex.

This study highlights the apex/crossing differences in terms of average direction angle of bedload particles in meander bends. Different particle direction angles for different size fractions arise from (7). Indeed, given the bed topography and stream flow condition, differential particle orientation takes place when the first term of the denominator of (7), which depends on particle size, from (5), becomes large compared to the second term of the denominator of (7). According to the analysis leading to (7), fine particles with high η_o move along the streamlines, coarse particles with low η_o have lower values of β and are expected to move toward the thalweg, thus resulting in sorting near the apex of meander bends. Conversely, near-horizontal bed surfaces with $\Theta_o=\Theta_1\cong 0$ give $\Theta\cong 0$ near meander crossings. One obtains from (7) that β is identical for all grain sizes because $a_\Theta\cong 1$ near meander crossings. As a result, no additional sorting should be obtained near meander crossings in the sense that particles of different sizes should move in near-parallel directions. Let us consider the measurements taken in the Fall River, Colorado, to compare average measurements with calculations.

3. Fall river study

3.1 Site selection

Fall River is a sinuous river flowing through the Horseshoe Park Area of Rocky Mountain National Park, Colorado. This river, with a drainage area of 90 km^2 at the study site (Fig. 2) has a simple yearly hydrograph. Peak snowmelt runoff during late spring exceeds bankfull flow for several weeks. After this snowmelt peak, discharge drops gradually to hit fall and winter lows. The bankfull flow of Fall River is about 7 m^3/s, and its winter lows are less than 0.5 m^3/s.

The Horseshoe Park area is a Pleistocene lake bed (Jarrett and Costa, 1985; Blair, 1987), giving Fall River a relatively gentle slope (0.0013) through the study reach. Upstream of the study site, the Horseshoe Park area features a unique alluvial fan. Coarse material recently formed this fan on July 15, 1982, after the failure of Lawn Lake dam located in the headwaters of Roaring River, a small tributary to Fall River (Pitlick, 1985). The alluvial fan acts as a major source of sediment for bedload transport to the study reach of Fall River.

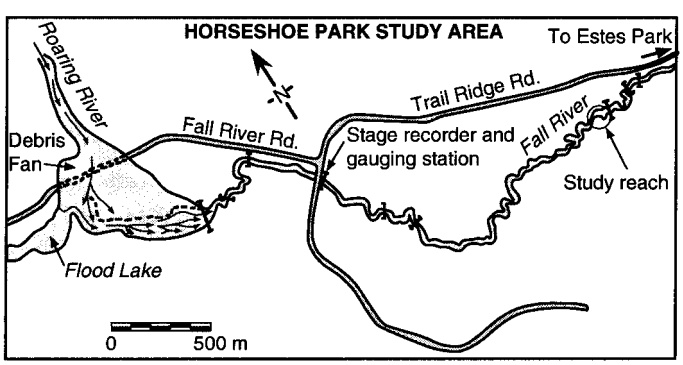

Fig. 2 Fall River location map

3.2 Instrumentation

During field seasons in 1986 and 1987, field measurements were taken along two consecutive Fall River bends (Anthony, 1992) to determine the patterns of internal cross-sectional adjustments which this river had undergone from high to low flows since the introduction of sediment from the alluvial fan (Anthony and Harvey, 1991). Field measurements included bed and free surface topography, velocity profiles and sediment transport by size fraction, with details in Anthony (1992).

At each cross-section, vertical velocity profiles were measured at one-meter intervals across the channel. A Marsh-McBirney current meter was used for the two-dimensional velocity measurements. Both transverse and longitudinal velocities were measured, starting from the bottom (with the current meter resting on the bottom) and then at approximately 10 cm intervals to the water surface. At each point in the profile, a 30-second sampling duration was allowed for measuring each velocity component. This sampling duration was extended to one minute or more when turbulence was significant (i.e. when the current meter showed instantaneous values of ± 0.1 m/s. A sampling error up to a few percent is expected from the surveys.

Sediment transport in the layer 0 to 7.67 cm above the bed was measured with a Helley-Smith sampler. Two one-minute bedload samples were taken at each vertical of each cross-section and the measurements were repeated three times. Note that the term bedload is used in a broad sense to designate near-bed sediment transport captured by the Helley-Smith sampler in the zone 0 to 7.67 cm above the bed. Sediment loads as high as 0.6 kg/m-s have been measured using a Helley-Smith sampler, with moving sediment fractions ranging from 0.125 to 32 mm.

3.3 Data collection program

In this study reach, 22 cross-sections were surveyed in 1986 at four different flow levels: rising stage, high flows of bankfull or greater discharge, falling stage, and low flows. Field measurements from 1986 show the overall flow pattern over the entire reach, but replicate measurements over specific sites in 1987 allow better calculations for testing the particle stability analysis. During the second field season in 1987, selected cross-sections (14, with nine near the bend apex) were repeatedly sampled (three to four times) at each flow level to investigate variability in the data sets. At each cross-section, measurements were taken along verticals spaced at 1 m intervals. Replicate measurements at each vertical included at least three velocity profiles (for both longitudinal and transverse flow) and six one-minute bedload measurements. This replication of measurements occurred during relatively stable flow conditions with most discharge varying between 2.5 and 3.5 m^3/s. The nine bend cross-sections were best suited to verify the calculations because bends have both cross-stream slope and cross-stream helical flow. Near stream crossings, both λ and θ_1 are 0° and hence β is expected to be 90° for all grain sizes, which indicates that all size fractions move in the downstream direction along near-parallel lines.

The channel bottom topography was also stable during this period with bed elevations usually varying by less than 10 cm between successive surveys. Small dunes reaching 10-25 cm in amplitude covered about 40% of the channel bed and generated small topographic irregularities. The average bed elevation of 3 to 4 surveys were used in the calculations. Overall, the channel has a fairly flat downstream slope $\Theta_o=0.0074^\circ$, or $\tan\Theta_o=0.0013$, and the channel bed side slope angle ranges from 0° at the crossings to 25° near the bend apex.

3.4 Results

Under high discharges, the cross-sectional geometry of this meandering channel alternates between a relatively rectangular shape at crossings to the most asymmetrical form near the bend apex as shown in Figure 3a. Near the apex, the characteristic shape features: 1) a deep thalweg along the outside of the bends; 2) a point bar platform along the inside of the bends; and 3) a point bar slope connecting the two.

The streamline deviation angle λ is obtained from the two-dimensional velocity measurements made near the channel bed. Both the velocity measurements close to the bed and those 10 cm above the bed were available for analysis. Both worked well, but there was more variability in magnitude and direction of the velocity measurements made at the bed, due to fluctuations caused by the large velocity gradient near the bed. The measurements made 10 cm above the bed showed a more consistent pattern of flow direction and magnitude, and are used to determine the streamline deviation angle λ, the direction of the velocity vector at 10 cm above the bed is shown in Figures 3b and 3c.

Total bed shear stress τ is often divided into grain shear stress τ', and bedform shear stress τ'' (Einstein and Barbarossa, 1952; Simons and Senturk, 1992; Richardson et al, 1990; Julien, 1995). One way to separate grain from total shear stress has been outlined by Dietrich and Whiting (1989). Their method determines grain shear stress from the measured velocity profile in a sand-bed river. It assumes a logarithmic velocity profile, and a y_o value elevation above the bed (where the extrapolated logarithmic velocity goes to 0) which is assumed equal to 10% of the d_{84} at the channel bed. The grain shear stress values obtained using the Dietrich and Whiting method at each sampling vertical are shown in Figure 3b. The orientation of the vectors in Figures 3b and 3c indicates the flow direction at a distance of 10 cm above the bed. For comparisons, the shear stress calculated from $\tau_w=\gamma h S_w$, using the local flow depth h and the reach-averaged water surface slope S_w, are shown in Figure 3c. Notice the difference in scale and magnitude of grain shear stress compared to the τ_w approximation. This shear stress τ_w is approximately equal to the total bed shear stress at least near the crossings and is hereafter referred to as the DuBoys shear stress.

Bedload measurements at each sampling location were sieved to determine the particle size distribution of moving material. Grain size distributions from replicate measurements were quite similar. Measured near-bed sediment movement at each sampling location was divided into weights for each size fraction. At each cross-section, the sediment movement for each size fraction was then summed over the entire cross-section. The magnitude of the

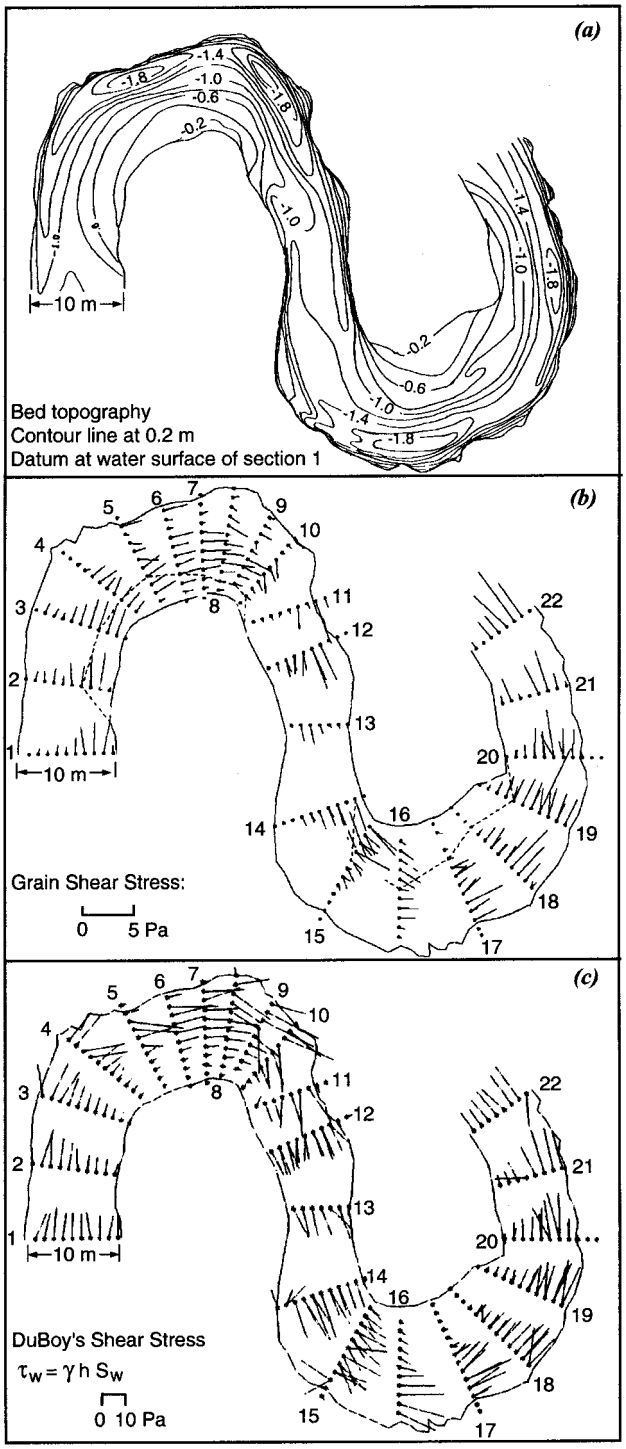

Fig. 3 a) bed topography at high discharge; b) grain shear stress; and c) total shear stress, each vector is oriented along the streamline measured 10 cm above the bed

sediment load varied slightly with discharge during the 1986 and 1987 surveys. The distribution of sediment load over cross-sections, however, was independent of discharge. For a given grain size, the percentage of the cross-section total material transported is then calculated for each sampling point. After repeating this process at each cross-section, a bedload percentage map over the entire reach is obtained for that particular size fraction. Bedload percentage maps were then produced for each size fraction, i.e. 16, 8, 4, 2, 1, 0.5, 0.25 and 0.125 mm. Typical bedload percentage maps are shown in Fig. 4 to represent coarse grains in transport ($d_{95} \cong 8$ mm), median grain size ($d_{50} \cong 1$ mm) and fine grains in transport ($d_{10} \cong 0.25$ mm). The sum of bedload percentages over each cross-section is always 100% for each size fraction.

The values of bedload percentages at each cross-section were used to calculate the position of the center of mass of bedload transport for each size fraction. It is interesting to note in Figure 4 that the location of the center of mass for fine grains is different from that of coarse grains. The lines linking the successive positions of the center of mass for different grain sizes are shown in

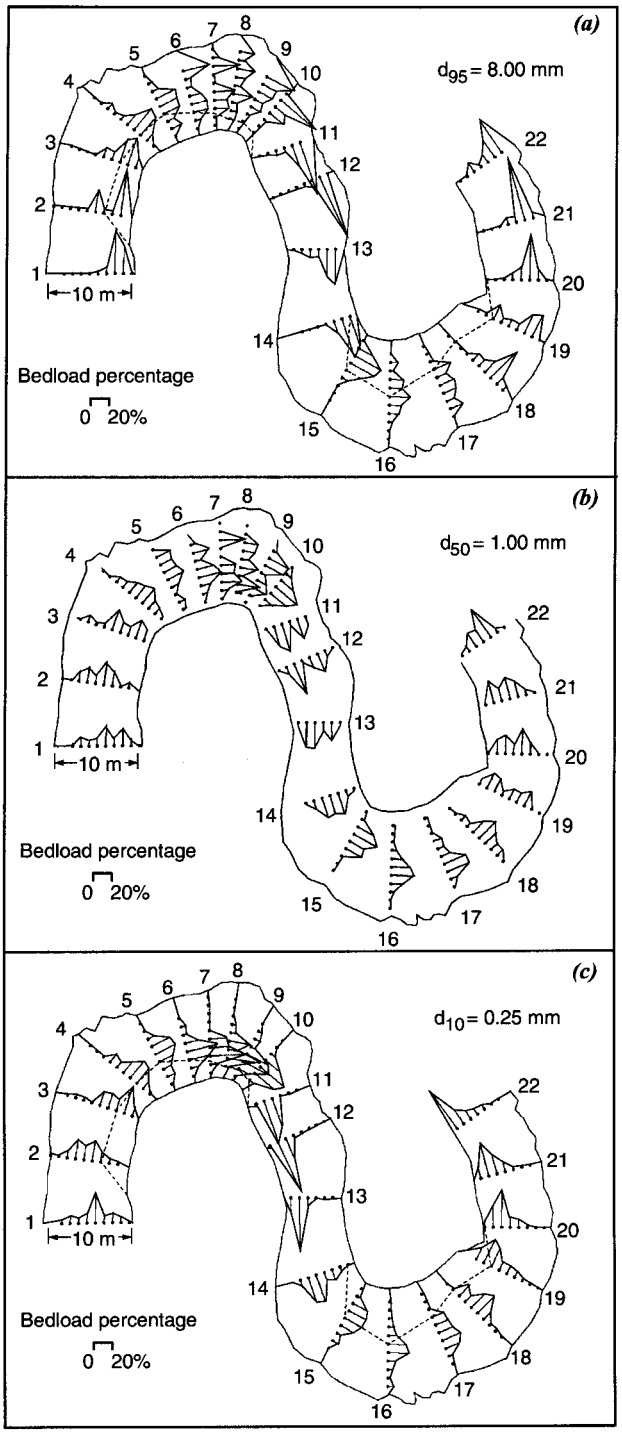

Fig. 4 Percentage of moving bedload at each interval for all channel cross-sections: a) d_{95}=8 mm; b) d_{50}=1.0 mm; and c) d_{10}=0.25 mm

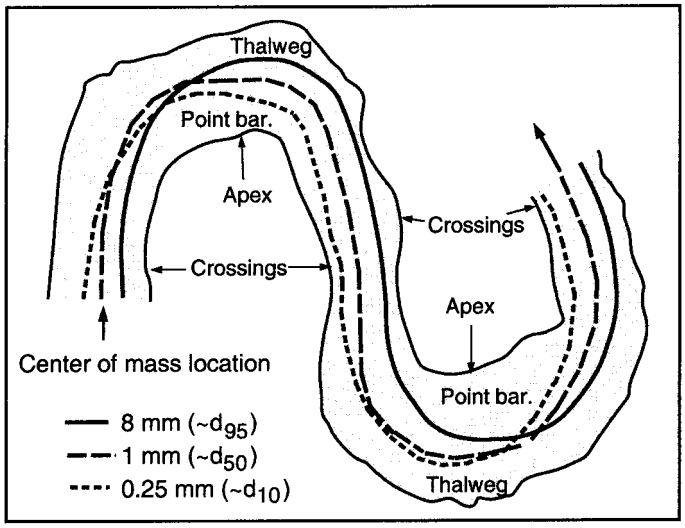

Fig. 5 Center of mass curves for three bedload size fractions

Figure 5. These can be considered as median trajectory maps for each grain size. The position of the center of mass for each size fraction shifts across the channel, and the net direction of sediment movement is different for each size fraction (Figs. 4 and 5). These figures present unique information on near-bed sediment transport by individual size fractions. It is interesting to observe that, near the meander crossing, the bedload center of mass curves for each size fraction are fairly parallel and oriented in the downstream direction, as expected from the calculations. On Figure 5, the measured particle orientation angle β between the tangent to the center of mass curve of moving sediment and the downstream direction will be used to test the calculations from (7).

4. Comparison with theoretical results

The Fall River data set contains sufficient information to test the main features of the aforementioned particle stability analysis in terms of the mean particle direction angle β calculated by size fraction, given the particle diameter, side-slope angle, downstream slope angle, streamline deviation angle at 10 cm above the bed, and the grain and total shear stresses in Figures 3b and 3c respectively. The grain shear stress in Figure 3b is quite comparable to the pattern of near-bed sediment transport shown in Figure 4. However, the magnitude of grain shear stress does not exceed 5Pa and cannot explain the motion of 32 mm particles. The magnitude of the total shear stress in Figure 3c however seemed more appropriate to describe near-bed sediment transport because the total shear stress is sufficiently large to move 32 mm particles. It is thus inferred that the total shear stress is a better description of the magnitude of shear stress while the grain shear is a better descriptor of the spatial distribution of shear stress in meander bends.

Since the Fall River data set includes flow depth, water surface slope, vertical velocity profiles, dune geometry and grain size distribution, the particle direction angle calculated from both grain and total shear stress are compared with field measurements. Field measurements consist of the orientation angle β of the center of mass curves from Figure 5. For each size fraction, the orientation angle β measured near apex cross-sections is compared with the average calculated orientation angle β at cross-sections 4,5,6,8,9,16 and 17. The results of calculations with both grain shear stress and total shear stress are plotted in Figure 6. A calculation example for typical near-apex conditions is shown in Appendix I. Values of β=90° correspond to the downstream direction, β<90° indicate motion toward the thalweg and β>90° indicates motion toward the point bar.

As expected, Figure 6 shows that sand particles tend to move to the point bars while gravel particles move toward the thalweg. The calculations using grain shear stress show calculated sediment angles much lower than the measured values. The calculated results with the methods of Dietrich and Whiting compare well with the calculations using the method of Limerinos (1970).

The Dietrich-Whiting method provides grain shear based on near-bed velocity measurements and d_{84} of the bed material. The method assumes a logarithmic velocity profile and a y_0 value equal to 0.1 d_{84}. This method gave values of the grain shear stress which were about 20% of the total average bed shear stress as shown in Figures 3b and 3c. The method of Limerinos (1970) was also used to double-check the magnitude of the grain shear stress. The Limerinos procedure provides grain shear stress $\tau' = \frac{f'}{8} \rho V^2$ where f' is the grain Darcy-Weisbach friction factor calculated from the hydraulics radius and the d_{84} of the bed material; ρ is the mass density of water and V is the depth-averaged flow velocity. The method of Limerinos gave values of the grain shear stress about 20% of the total shear stress and the results on Figure 6 are very comparable to those of Dietrich and Whiting.

Figure 6 also shows the results of calculations using the total shear stress. Two methods of calculating the total shear stress were used; the DuBoys method with shear stress distribution shown in Figure 3c; and 2) the shear stress calculated using van Rijn's method. The method of DuBoys is based on average downstream slope and local flow depth. The method of van Rijn (1984)

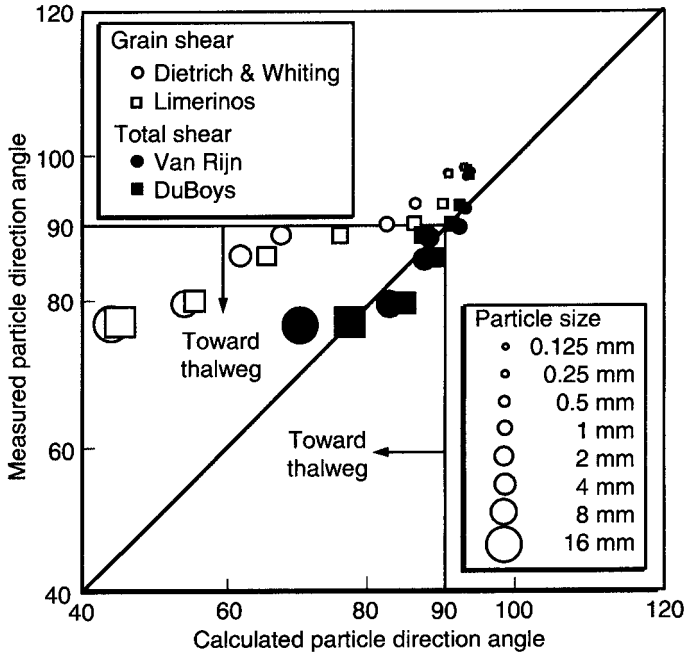

Fig. 6 Near-apex vs measured calculated particle direction angles

calculates the total grain roughness parameter k_s from $k_s = 3\ d_{90} + 1.1\ \Delta\ (1\text{-}e^{-25\Delta/\Lambda})$ using the measured bed form height Δ, bedform length Λ and d_{90} of the bed material. The results of van Rijn's shear stress calculations were about 80% of the DuBoys calculations, but were different in spatial distribution. The bedload particle orientation angles calculated using the total shear stress were in very good agreement with the measured values shown in Figure 6. The agreement between calculated and measured particle deviation angles is sufficiently good to demonstrate that on the average, fine particles move toward the point bars, while coarse particles move toward the thalweg of sinuous sand and gravel bed channels.

In the sharp meander bends of Fall River, there is a 22° angle difference between the average direction of coarse and fine particles moving near the bed. In this case, coarse gravel particles (d_{97}=16 mm) move at an average angle of about 13° toward the thalweg of the meandering channel. At the same time, fine sand (d_5=0.125 mm) moves at an average angle of about 9° toward the point bar. Figure 7 shows comparison between near-apex and near-crossing results. The method of van Rijn is used in both sets of calculations. This figure shows that the particle direction angle is approximately the same for all size fractions near stream crossings. It can be inferred that grain sorting does not take place in the fairly straight reaches near the meander crossing. Conversely, the bedload center of mass curves are very different for each size fraction near the bend apex. This is the zone where grain sorting occurs due to the angle difference between coarse and fine grains.

5. Summary and conclusions

A three-dimensional particle stability analysis is presented with application to the determination of the average near-bed particle direction angle in the sharp meander bends of Fall River, Colorado. The analysis of moments applied to a particle yields a particle stability factor SF_0 in (3) from calculations of the plane bed stability number η_0 (5), the particle direction angle β (7), and the sideslope stability number η_1 (4). An example of the calculation procedure is given, along with application of the method to determine the direction of bedload motion by size fractions in the sharp meander bends of the Fall River. Grain sorting can be directly calculated from (7) because $\eta_o \tan \phi$ varies with grain size. The analysis of a unique field data set of near-bed sediment transport by size fractions 0.125 mm<d_s<32 mm using a Helley-Smith sampler indicates local variability in calculated particle orientation angle according to (7). Grain sorting can be satisfactorily calculated as shown in Figure 6 from bed topography, two-dimensional velocity direction measurements taken 10 cm above the bed and total shear stress estimates based on the product of local flow depth and reach-averaged friction slope. The measured particle orientation angle from the center of mass curves in Figure 4 is comparable to the average particle direction angle calculated for each size fraction (Fig. 7). The results indicate that an angle of about 20° separates the average direction of coarse gravel and fine sand near the apex of the sharp meander bends of the Fall River. Within a bend, coarse gravel particles move from the inner bank toward the outer bank while fine sand particles move from the outer bank toward the inner bank. Near meander crossings, the center of mass of fine and coarse particles follow near-parallel trajectories.

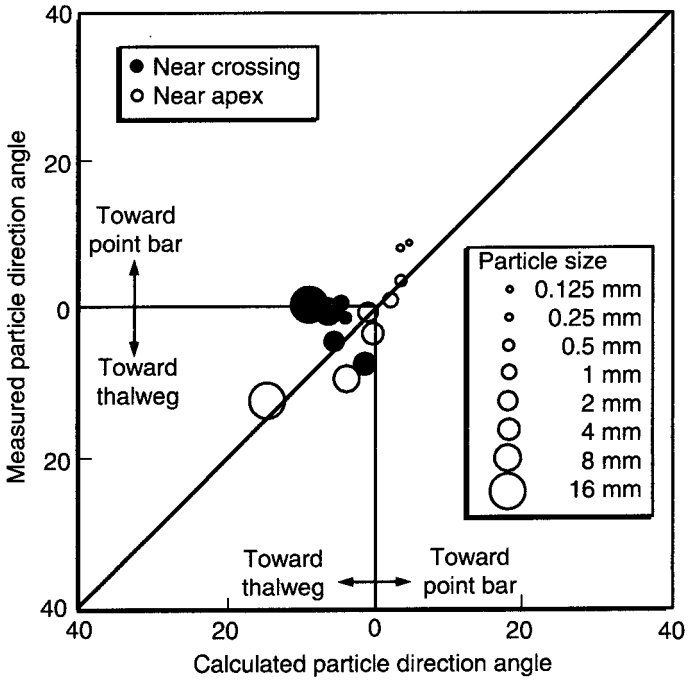

Fig. 7 Near-apex vs near-crossing measured and calculated particle direction angles

6. Acknowledgments

The authors are grateful to S. Schumm and M. Harvey for their input and guidance on the Fall River portion of the research, and to J. Pitlick for his invaluable field assistance. Funding for portions of this research has been granted by the National Park Service and the Army Research Office (ARO/DAAL 03-86-K-0175 and ARO/DAAL 04-94-G-0420). This work was supported by the Department of Defense Center for Geosciences/Atmospheric Research Agreement #DAAL01-98-2-0078.

References

ANTHONY, D.J., 'Bedload transport and sorting in meander beds, Fall River, Rocky Mountain National Park, Colorado', Ph.D. Dissertation, Dept. of Earth Resources, Colorado State University, Fort Collins, CO, 1992.

ANTHONY, D.J. and M.D. HARVEY, 'Stage-dependent cross-section adjustments in a meandering reach of Fall River, Colorado.' Geomorphology, Vol. 4: 187-203, 1991.

BLAIR, T.C., 'Sedimentary processes, vertical stratification sequences, and geomorphology of the Roaring river alluvial fan, Rocky Mountain National Park, Colorado.' J. Sed. Petrology, Vol. 57: 1-18, 1987.

BROOKS, N.H., discussion on 'Boundary shear stress in curved trapezoidal channels'. J. Hydr. Engrg., ASCE, 89(3), 327-333, 1963.

DIETRICH, W.E. and P.J. WHITING, 'Boundary shear stress and

sediment transport in river meanders of sand and gravel.' In River Meandering, AGU Water Resources Monograph, Washington, DC, 1-50, 1989.

DUBOYS, M.P., 'Etude du régime du Rhône et de l'action exercée par les eaux sur un lit à fond de graviers indéfiniment affouillable,' Annales des Ponts et Chaussées, Ser. 5, Tome 18, No. 49, 141-195, 1879.

EGIAZAROFF, I.V., 'Calculation of non-uniform sediment concentration.' J. Hydr. Div., ASCE, 91(HY4): 225-248, 1965.

EINSTEIN, H.A. and N.L. BARBAROSSA, 'River channel roughness.' Trans., ASCE, v. 117, 1121-1146, 1952.

ENGELUND, F., 'Flow and bed topography in channel bends.' J. Hydr. Div., ASCE, 100(HY11): 1631-1648, 1974.

HAYASHI, T., S. OZAKI and T. ISHIBASHI, 'Study on the bedload transport of sediment mixture.' Proc. 24th Japanese Hyd. Conf., pp. 35-43, 1980.

IKEDA, S., 'Lateral bedload on side slopes.' J. Hydr. Div., ASCE, 108(HY11), 1369-1373, 1982.

JARRETT, R.D. and J.E. COSTA, 'Hydrology, geomorphology and dam-break modeling of the July 15, 1982 Lawn Lake dam and Cascade Lake dam failures, Larimer County, Colorado.' USGS Open File Report, 84-612, 109 p, 1985.

JULIEN, P.Y., Erosion and Sedimentation, Cambridge University Press, NY, 280 p., 1995.

KAWAI, S. And P.Y. JULIEN, 'Point bar deposits in narrow sharp bends,' J. Hydr. Res., IAHR, 34(2), 205-218, 1996.

KOCH, F.G. and C. FLOKSTRA, 'Bed level computations for curved alluvial channels,' Proc. XIX Congress of the IAHR, Vol. 2, New Delhi, India, p. 357, 1980.

KOVACS, A. and G. PARKER, 'A new vectorial bedload formulation and its application to time evolution of straight river channels,' J. Fluid Mech., 267, 153-183, 1994.

KUHNLE, R.A., 'Incipient motion of sand gravel sediment mixtures.' J. Hyd. Div., ASCE, 119(HY12): 1400-1415, 1993.

LANE, E.W., 'Progress report on studies on the design of stable channels by the Bureau of Reclamation', Proc., ASCE, No. 280, Sept, 1953.

LIMERINOS, J.T., 'Determination of the Manning coefficient for measured bed roughness in natural channels,' USGS Water Supply Paper 1891-B, 47 p., 1970.

ODGAARD, A.J., 'Transverse bed slope in alluvial channel bends.' J. Hydr. Div., ASCE, 107(HY12), 1677-1694, 1981.

ODGAARD, A.J., 'Bed characteristics in alluvial channel bends.' J. Hyd. Div., ASCE, 108(HY11), 1268-1281, 1982.

PARKER, G. and E.D. ANDREWS, 'Sorting of bedload sediments by flow in meander bends.' Water Resour. Res., AGU, 21(9), 1361-1373. 1985.

PITLICK, J.C., 'The effect of a major sediment influx on Fall River, Colorado.' M.S. Thesis, Dept. of Earth Resources, Colorado State University, Fort Collins, CO, 127 p, 1985.

RICHARDSON, E.V., D.B. SIMONS and P.Y. JULIEN, 'Highways in the River Environment', Training and Design Manual for the U.S. Dept. of Transportation, Fed. Highway Admin., Pub. No. FHWA-H1-90-016, February, 1990.

SHIELDS, A., 'Anwendung der Aehnlichkeitsmechanik und der Turbulenzforschung auf die Geschiebebewegung.' Mitteilungen der Preussische Versuchanstalt für Wasserbau und Schiffbau, Berlin, 1936.

SIMONS, D.B. and F. SENTURK, 'Sediment transport technology.' Water Resources Publications, Fort Collins, CO, 897 p. 1992.

STEVENS, M.A. and D.B. SIMONS, 'Stability analysis for coarse granular material on slopes,' Chap. 17 in River Mechanics, Water Resources Publications, Fort Collins, CO, 1971.

STRUIKSMA, N., K.W. OLESEN, C. FLOKSTRA, and H.J. de VRIEND, 'Bed deformation in curved alluvial channels.' J. Hydr. Res., IAHR, 23(1), 57-79, 1985.

TALMON, A.M., M.C.L.M. van MIERLO, and N. STRUIKSMA, 'Laboratory measurements of the direction of sediment transport on transverse alluvial-bed slopes.' J. Hydr. Res., IAHR, 22(4), 495-517, 1995.

van RIJN, L.C., 'Sediment transport part III: Bedforms and alluvial roughness,' J. Hydr. Div., ASCE 110(12), 1733-1754, 1984.

WHITING, P.J. and W.E. DIETRICH, 'Boundary shear stress and roughness over mobile alluvial beds.' J. Hydr. Div., ASCE, 116(9), 1495-1511, 1990.

YALIN, M.S. and E. KARAHAN, 'Inception of sediment transport', J. Hydr. Div., Proc., ASCE, 105(HY11): 1433-1443, 1979.

YEN, C.L. and K.T. LEE, 'Bed topography and sediment sorting in channel bend with unsteady flow.' J. Hydr. Engrg., ASCE, 121(8), 591-599, 1995.

Notation

a_Θ	geometric coefficient
d_s	grain diameter (d_{90} represents the size for which 90% by weight is finer)
f_s	coefficient in van Bendegom's weight function
f'	grain Darcy-Weisbach friction factor
F_B	buoyancy force
F_D	drag force
F_L	lift force
F_S	submerged particle weight
F_W	particle weight
g	gravitational acceleration
G	specific gravity of sediment
h	flow depth
k_s	total grain roughness parameter
$\ell_1, \ell_2, \ell_3, \ell_4$	moment arms in particle stability analysis
M	moment ratio of lift to submerged weight
N	moment ratio of drag to submerged weight
r_c	radius of curvature of a meander bend
$Re^* = U_* d_s / \upsilon$	grain shear Reynolds number
S_W	free surface slope
SF_0	stability factor against rotation about 0
$U_* = \sqrt{g h S}$	shear velocity
V	depth-averaged flow velocity
y_0	reference elevation in Dietrich-Whiting method
β	particle direction angle
γ	specific weight of water

Δ dune height
δ angle between streamline and particle directions
η_0 plane bed stability number
η_1 side slope stability number
Θ angle with vertical plane
Θ_0 downstream bed slope angle
Θ_1 side slope angle
Λ dune length
λ streamline deviation angle
ρ,ρ_s mass density of the fluid and sediment particle respectively
ϕ bed material angle of repose
τ_o,τ_o',τ_o'' bed shear stress, respectively total, grain and bedform
τ_c critical shear stress
τ_w shear stress calculated from free surface slope
τ_* Shields parameter
τ_{*c} critical Shields parameter

Appendix I - Practical considerations and example

The following example details the calculation of particle stability for typical conditions in the Fall River using (3), (4), (5), and (7). The analysis shows that the calculated orientation angle β depends on M/N. Theoretical research is indicated for better evaluation of M/N for different particle sizes. However, given all the data at each cross-section, there is an overall difference of a few degrees between the calculated angles β using M/N=0 instead of M/N=1. The overall agreement with field data being slightly better with M/N=0, this value was given preference for all calculations.

A 16 mm quartz particle stands on the bed of a channel under 1 m of water, if the downstream channel slope angle is Θ_o=0.074° and the side slope angle is Θ_1=15°, calculate the particle direction angle under an applied shear τ_o=12 Pa when the streamlines are deflected upward at λ=-10°. Notice that the applied shear roughly corresponds to

$$\tau_w = \gamma h S_W = \frac{9810\ N}{m^2} \text{ x } 1 \text{ m x } \tan 0.074° = 12 \text{ Pa}$$

given a flow depth h≅1 m and $S_W \cong \tan \theta_0$. The calculation procedure follows:

i) the particle size is d_s=16 mm
ii) the angle of repose is approximately ϕ=37°, and the specific gravity G=2.65
iii) the side slope angle is Θ_1=15°
iv) the downstream slope angle is Θ_0=0.074°
v) the angle $\Theta=\tan^{-1}(\sin\Theta_0/\sin\Theta_1)$=0.28°
vi) the geometric factor $a_\Theta = \sqrt{\cos^2\Theta_1 - \sin^2\Theta_0} = 0.965$
vii) the applied stream stress is τ_o=12 Pa
viii) the streamline deviation angle λ=-10° means that the downstream shear stress component is $\tau_o \cos\lambda$=11.8 Pa and the transverse shear stress is $\tau_o \sin\lambda$=-2.08 Pa toward the free surface (negative)
ix) From (5) and τ_{*c}=1/21, the plane bed stability number is,

$$\eta_0 = \frac{12\ N\ m^3\ s^2\ 21}{m^2\ (1.65)\ 1000\ kg\ x\ 9.81\ m\ x\ 0.016\ m} = 0.97$$

x) From (7), the 16 mm particle direction angle is

$$\beta = \tan^{-1}\left[\frac{\cos(-10° + 0.28°)}{\frac{\sqrt{1 - (0.965)^2}}{0.97\tan 37°} + \sin(-10° + 0.28°)}\right] = 79°$$

xi) The 16 mm particle moves toward the thalweg because $\beta + \Theta < 90°$

The calculations are repeated for the smallest particle d_s=0.125 mm under the same hydraulic conditions, τ_{*c} = 0.047 and ϕ=37°. It is found that the 0.125 mm particle direction angle β=99°. The 0.125 mm particle moves toward the point bar because β>90. Notice that there is approximately a 20° difference (99°-79°) between the direction of the 0.125 mm and the 16 mm particles under identical hydraulic conditions.